ACS Combinatorial Science

Research Article

pubs.acs.org/acscombsci

Composition–Structure–Function Diagrams of Ti–Ni–Au Thin Film Shape Memory Alloys

Pio John S. Buenconsejo*,‡ and Alfred Ludwig*

Institute for Materials, Ruhr-Universität Bochum, 44801 Bochum, Germany

ABSTRACT: Ti–Ni–Au thin film materials libraries were prepared from multilayer precursors by combinatorial sputtering. The materials libraries were annealed at 500, 600, and 700 °C for 1 h and then characterized by high-throughput methods to investigate the relations between composition, structure and functional properties. The identified relations were visualized in functional phase diagrams. The goal is to identify composition regions that are suitable as high temperature shape memory alloys. Phase transforming compositions were identified by electrical resistance measured during thermal cycles in the range of -20 and 250 °C. Three phase transformation paths were confirmed: (1) B2–R, (2) B2–R–B19′, and (3) B2–B19. For the materials library annealed at 500 °C only the B2–R transformation was observed. For the materials libraries annealed at 600 and 700 °C, all transformation paths were observed. High transformation temperatures ($M_s \approx 100$ °C) were only obtained by annealing at 600 or 700 °C, and with compositions of Ti ≈ 50 at. % and Au > 20 at. %. This is the composition range that undergoes B2–B19 transformation. The phase transformation behaviors were explained according to the compositional and annealing temperature dependence of phase/structure formation, as revealed by X-ray diffraction analysis of the materials libraries.

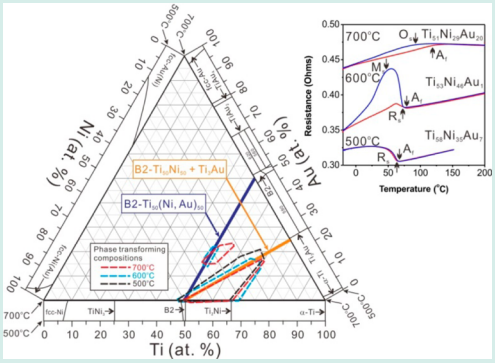

KEYWORDS: *thin films, annealing, high temperature shape memory alloys, combinatorial materials science, phase transformation*

INTRODUCTION

Shape memory alloy (SMA) thin film actuators have the advantage of a large work output when compared to other actuator materials, like PZT, due to their higher recovery force and larger transformation strain.[1] This is the main motivation for implementing SMA based actuators in microelectro-mechanical-systems (MEMS). Among the known SMAs the NiTi-based alloys are the most studied in bulk and thin film because of their excellent shape memory and mechanical properties. The addition of third elements has been extensively investigated in order to extend operating temperatures above room temperature. Typically martensite transformation start (M_s) temperatures >100 °C is desired for applications in transportation systems, heating systems and energy conversion-generation systems. Additionally, a high transformation temperature is effective to improve actuation frequency because of steeper cooling gradient. To raise the transformation temperatures, TiNi-bulk SMA is alloyed with noble metals,[2−4] such as Pt, Pd, and Au, or less expensive metals, such as Zr[5] and Hf.[6] Among them the least studied is the Ti–Ni–Au bulk SMA.[2−4,7−10] Each alloying elements have their pros and cons, with regards to cost, processing, oxidation resistance and functional stability, so the choice of alloying element largely depends on the proposed application. The noble metals offer smaller transformation hysteresis, when compared to alloying with Zr or Hf. In this regard Ti–Ni based SMA thin films alloyed with the noble metals are attractive for microactuator applications. The thin film properties of Ti–Ni–Pd[11−15] and Ti–Ni–Pt[15,16] SMA have already been reported but there are no published reports on Ti–Ni–Au SMA thin films.

Therefore, this paper investigates the Ti–Ni–Au system to identify the composition region and annealing condition required to obtain high transformation temperatures in the thin films. Combinatorial sputter-deposition of thin film materials libraries[17] and high-throughput experimentation[18] were employed in order to cover a wide composition range of the Ti–Ni–Au system and to perform efficient screening of desired properties. As a result composition-structure–functional property relations were established and visualized in a functional phase diagram. The important parameters for obtaining the desired functional properties can be readily derived from these diagrams.

EXPERIMENTAL PROCEDURES

Using a combinatorial sputter-deposition system (DCA Finland), Ti–Ni–Au thin film materials libraries were prepared via wedge-type multilayer sputter-deposition of Ti, Ni, and Au from elemental targets (with at least 99.9% purity). These libraries are continuous composition spreads of ternary mixtures deposited on SiO_2(1.5 μm)/Si substrate with 4-in. diameter. The oxide layer serves as a diffusion barrier during annealing. Each element was deposited as a thickness wedge

Received: May 2, 2014
Revised: August 12, 2014
Published: November 4, 2014

using a moveable shutter mask that moves at constant velocity. The wedges for each element were separated from each other by 120° rotation with respect to the substrate center. A multilayer stacking of Ti/Ni/Au precursor layers was repeated several times and a total thickness of at least >500 nm was achieved. A detailed description of the combinatorial sputter-deposition method can be found in ref 17 and in an animation (www.rub.de/wdm/forschung/projekte/videos.html.en). Composition mapping of the materials libraries was carried out in a scanning electron microscope (SEM, JEOL JSM 5800LV) with an Oxford INCA 250 system, consisting of the INCA X-act energy dispersive X-ray (EDX) detector and INCA-EDX software. Accuracy of composition measured by EDX was about 1−2 at. % of the measured value, so the compositions are rounded to the nearest integer. Measurement areas of 4.5 × 4.5 mm^2 separation were defined on the materials library. In some regions of the library 2.25 × 2.25 mm^2 separations were defined for higher resolution. Three Ti−Ni−Au thin film materials libraries with identical composition coverage were annealed in UHV at different temperatures (500, 600, 700 °C) for 1 h in order to induce alloying and phase formation. High-throughput screening to identify regions with phase transformation was performed by temperature-dependent electrical resistance (R(T)) measurements using a four-point probe setup during thermal cycling (heating/cooling rate of 5 °C) between -20 and 250 °C.[18] Phase formation after annealing was examined by X-ray diffraction (XRD) mapping analysis of each materials library using Cu−K_α as X-ray source (Panalytical Expert Pro, beam spot resolution of 3 mm × 5 mm). XRDsuite software[19] was used to facilitate the viewing and data analysis of a large amount of combinatorial XRD data sets. To confirm the consistency of the phase transformations observed in the R(T) screening, XRD(T) was performed on representative samples by using a heating/cooling stage (Anton Paar TTK450+LN2) attached in the XRD system.

RESULTS AND DISCUSSION

Phase Transforming Region. Figure 1 shows typical resistance−temperature (R(T)) curves of phase transforming compositions measured in the Ti−Ni−Au materials libraries which were annealed at different temperatures. The transformation temperatures were determined by the tangential method and indicated by arrows in the $R(T)$ plot. The phase transforming region measured within the temperature range of -20 and 250 °C revealed three different types of $R(T)$ curves indicating phase transformations of the types B2−R (Figure 1a), B2−R−B19′ (Figure 1b), and B2−B19 (Figure 1c). Nontransforming compositions show no sharp inflection in their $R(T)$ curves, as shown in Figure 1d. The observed shapes of the $R(T)$ curves are all consistent with previous results for other ternary and quaternary Ti−Ni based SMA thin films.[20−24]

The B2 phase is the parent phase, while the different martensite products are the R phase (trigonal martensite), B19 (orthorhombic martensite), and B19′ (monoclinic martensite). The reversible structural transformation paths were confirmed by XRD(T) on representative samples (Figure 2). The B2−R transformation is typically characterized by a narrow hysteresis in its $R(T)$ curves. The structure change observed by XRD is confirmed as the appearance and disappearance of (110)B2 and (300)R peaks. The B2−R−B19′transformation is a two stage transformation where the first stage is the B2−R transformation and then R-B19′transformation follows. Typically transformation to B19′ martensite is characterized by a wide hysteresis.

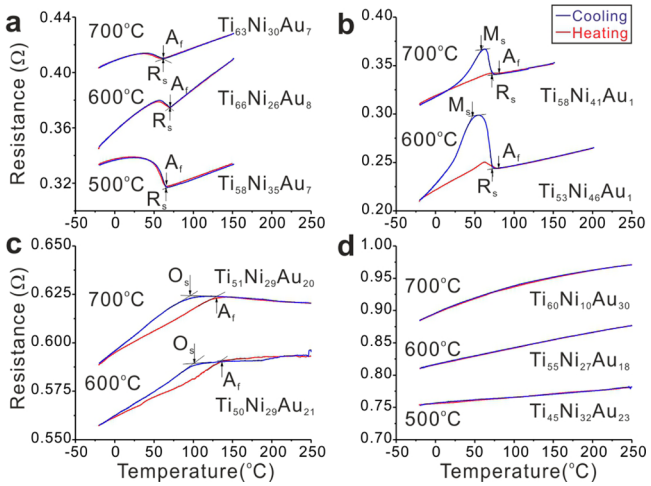

Figure 1. Typical $R(T)$ curves observed in the three differently annealed Ti−Ni−Au thin film materials libraries: (a) B2−R transformation, (b) B2−R−B19′ transformation, (c) B2−B19 transformation, and (d) no phase transformation. The phase transformation temperatures are as follows: R_s (transformation start to R trigonal martensite), M_s (transformation start to B19′ monoclinic martensite), O_s (transformation start to B19 orthorhombic martesnite), and A_f (reverse transformation finish to B2 phase).

Similarly the structural transformation is confirmed from the appearance of two successive martensite structures (R then B19′) during thermal cycle. The last type of transformation is the B2−B19 transformation, and it is characterized by hysteresis, which is wider than the B2−R transformation, and it is single-stage. The structural transformation is confirmed by the appearance and disappearance of (110)B2 and (111)B19. It should be mentioned that in all the cooling and heating experiments the peaks due to precipitate phases (Ti_2Ni and Ti_3Au, fcc-Au) remained unchanged but only for small shifts attributed to thermal expansion and contraction of their lattice. This is an expected behavior of phases that do not undergo structural transformations.

A strong annealing temperature and composition dependence of the phase transformation behavior was confirmed. The results are summarized in Figure 3. The phase transformation path (Figure 3a) for the materials library annealed at 500 °C revealed only the B2−R transformation. For materials libraries annealed at 600 and 700 °C the B2−R, B2−R−B19′, and B2−B19 transformation paths were confirmed. For small grain size, the transformation to B19′ or B19 martensite phases is suppressed to lower temperatures, while R phase transformation is not affected.[38] The materials library annealed at 500 °C exhibits small grain size because of low annealing temperature, so it is one reason that B19′ and B19 phase transformation was not confirmed. The higher annealing temperature (>600 °C) results in bigger grain size, so it increases the transformation temperatures of B19′ and B19 phases. This is one reason for the appearance of B2−R−B19′ and B2−B19 phase transformations in materials libraries annealed at 600 and 700 °C. In general B2−R and B2−R−B19′transformations were found in the composition range from Ti near 50 at. % and it extends toward the Ti-rich side with increasing Au content. The compositions with B2−R−B19′ transformation were confirmed in the region with Au <5 at. %, and the composition range slightly widened with higher annealing temperature. The compositions with B2−B19

dx.doi.org/10.1021/co5000745 | ACS Comb. Sci. 2014, 16, 678−685

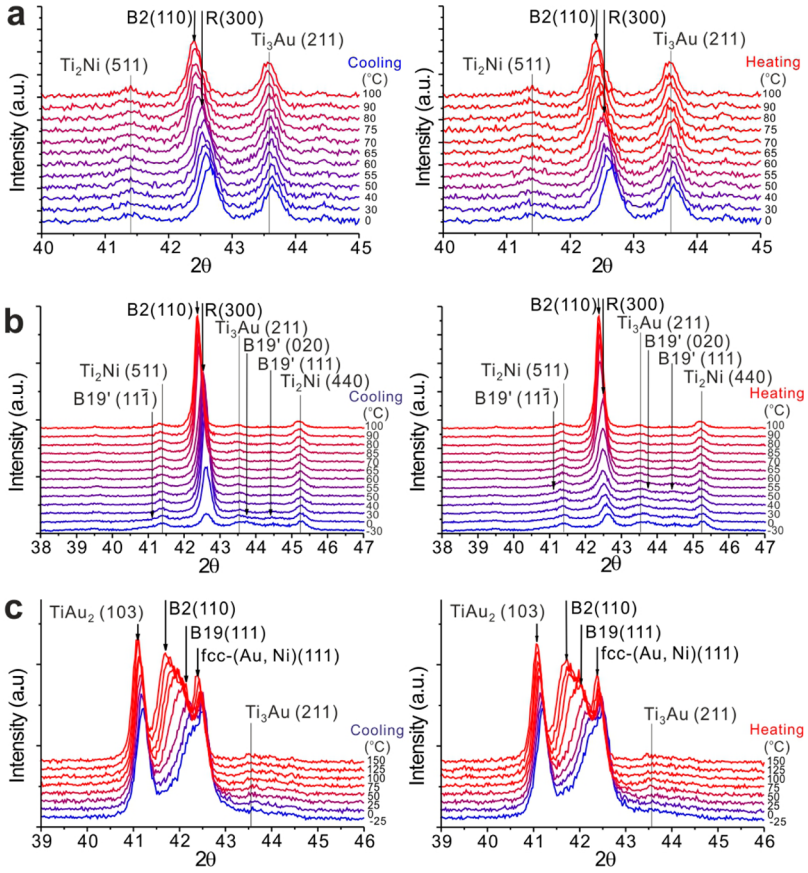

Figure 2. Representative XRD(T) patterns for (a) B2−R trigonal martensite ($Ti_{68}Ni_{18}Au_{14}$), (b) B2−R−B19′ monoclinic martensite ($Ti_{56}Ni_{42}Au_2$), and (c) B2−B19 orthorhombic martensite ($Ti_{50}Ni_{34}Au_{16}$) structural transformations confirmed in the materials library.

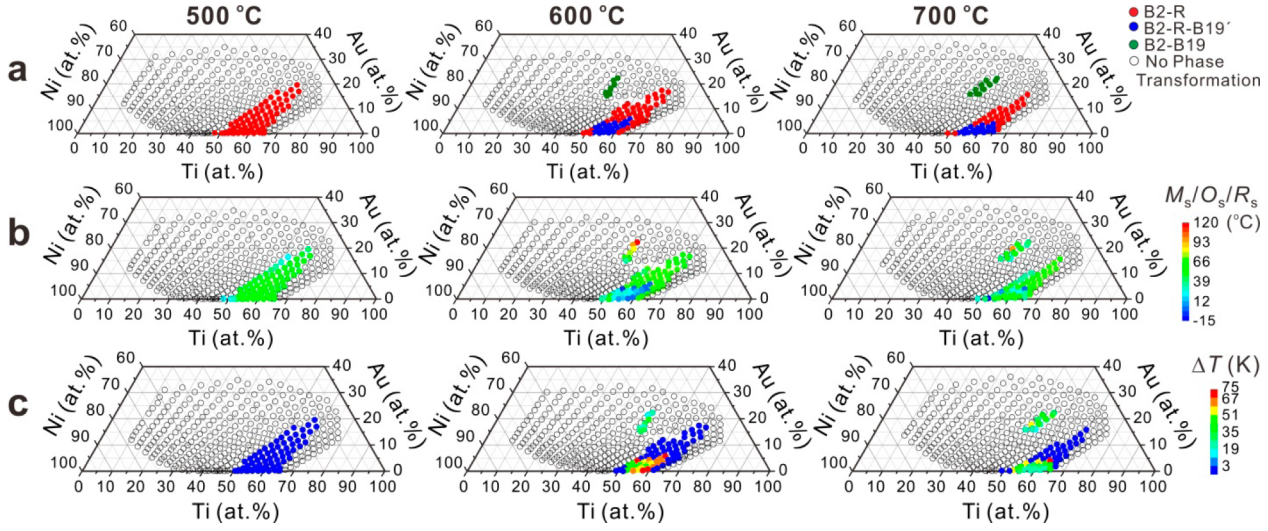

Figure 3. Phase transformation behavior observed in three Ti−Ni−Au materials libraries, which were annealed 500, 600, and 700 °C, respectively. (a) Types of phase transformations as confirmed by $R(T)$ in the range of −20 and 250 °C, (b) phase transformation start ($O_s/M_s/R_s$) temperatures, and (c) transformation hysteresis (ΔT) computed as the difference between A_f and transformation start (M_s or O_s or R_s) temperature. Color-coded legend and scales are shown on the right.

transformation were confirmed near Ti ≈ 50 at. % and Au in the range of 15 to 24 at. %. This region is very narrow and completely separated from the composition region undergoing B2−R and B2−R−B19′ phase transformations. Two interesting points from these results are (1) the appearance of two separate regions of phase transforming composition boundaries within the materials libraries annealed at 600 and 700 °C and (2) the location of the phase transforming boundaries with respect to composition. These results also show the high reproducibility of the observed effects. The underlying mechanism is discussed (Relationships between Phase Formation and the Phase Transforming Region section) with respect to the alloying behavior of Ti−Ni−Au thin film materials libraries.

dx.doi.org/10.1021/co5000745 | ACS Comb. Sci. 2014, 16, 678−685

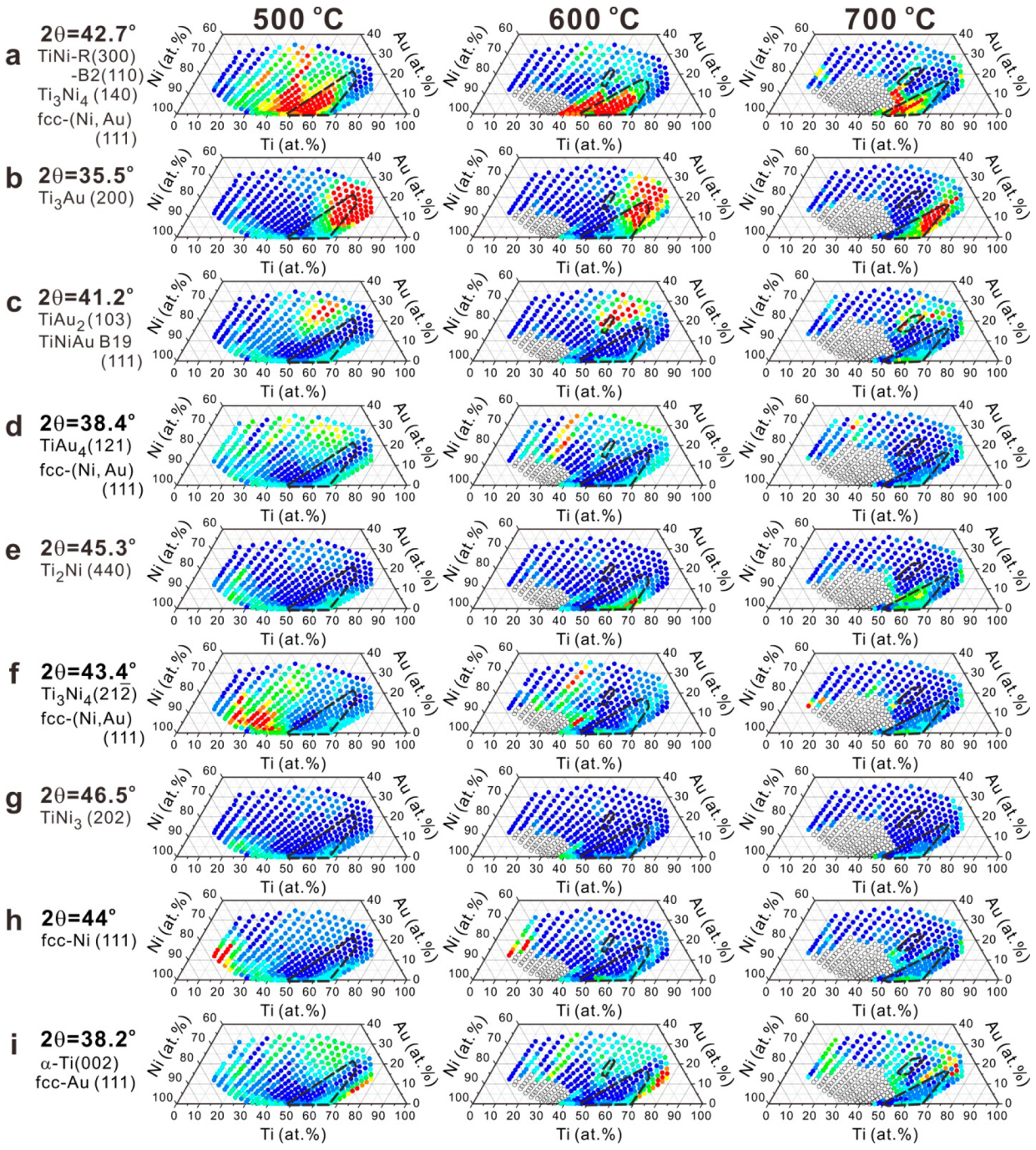

Figure 4. Color-coded peak intensity profile of phases confirmed by XRD analysis of materials libraries annealed at different temperatures: (a) TiNi R, B2, fcc-(Ni,Au), Ti_3Ni_4; (b) Ti_3Au; (c) $TiAu_2$, TiNiAu B19; (d) $TiAu_4$, fcc-(Ni,Au); (e) Ti_2Ni; (f) Ti_3Ni_4, fcc-(Ni,Au); (g) $TiNi_3$; (h) fcc-Ni; (i) α-Ti, fcc-Au. The color gradient red, green and blue correspond to high, medium and low peak intensity, respectively. Dashed black lines indicate the phase transforming composition regions.

The transformation start temperatures due to R phase (R_s), B19′ phase (M_s), and B19 phase (O_s) are plotted in Figure 3b. For compositions that undergo the B2−R−B19′ transformation, only the transformation temperature related to B19′ (M_s) is plotted. The M_s is relatively low (<60 °C) while R_s is higher, but it never reached more than 75 °C. The highest transformation temperature was realized for compositions with B19 transformation (Ti ≈ 50 at. % and >20 at. % Au), where O_s reached >100 °C.

Phase transformation hysteresis values ($\Delta T = A_f - M_s$ or R_s or O_s) as a function of composition are plotted in Figure 3c. The compositions undergoing B2−R transformation exhibited a very small ΔT < 3 K. For some compositions they exhibited *zero* hysteresis behavior, which is associated with the physical-mechanical constraint (such as the substrate or large amount of precipitates) effect on a phase transforming material.[23,25−28] The compositions undergoing a two-stage transformation from B2 to R and successively to B19′ martensite, exhibited higher hysteresis values (ΔT > 30 K) that is consistent with the wide ΔT observed typically for transformation to B19′ martensite. Compositions undergoing the transformation from B2 to B19 martensite have intermediate ΔT values from 20 to 45 K, which

dx.doi.org/10.1021/co5000745 | ACS Comb. Sci. 2014, 16, 678−685

is also consistent with values reported for bulk Ti−Ni−Au SMA.[4]

Phase Formation in Ti−Ni−Au Materials Libraries Annealed at Different Temperatures. Phase constitution over different compositions in the materials library was mapped by XRD analysis at room temperature. The phases were identified with reference to data acquired from Pearson Crystal Data: Crystal Structure Database for Inorganic Compounds.[29] The following phases were confirmed: the phase-transforming phases (B2, B19, R phase), Ti−Au intermetallic phases (Ti_3Au, $TiAu_2$, $TiAu_4$), Ti−Ni nontransforming intermetallic phases (Ti_2Ni, Ti_3Ni_4, $TiNi_3$), fcc-(Au, Ni) solid solution, and α-Ti phase. To identify phase stability regions of each phase the diffraction peak that best identifies the phase is selected and its intensity is plotted in a ternary composition diagram.[22] The peak intensity plots for all the phases identified are shown in Figure 4. In some cases the diffraction peak of various phase overlaps (or very close to each other) at the same diffraction angle (2θ). This leads to convolution of diffraction peaks from several phases. For this case, the peak intensity profile is a superposition of peak intensity contributions from several phases at the specific diffraction angle.

The compositions with Ti < 48 at. % did not show any phase transformation since they were dominated mainly by a mixture of various phases, such as fcc-Ni(Au), Ti_3Ni_4, and $TiNi_3$. Furthermore, with increasing annealing temperature a large number of compositions in the Ti poor region peeled off from the substrate (shown with no color code), which is most probably due to the high thermal and physical mismatch of mixed phases and the substrate. On the other hand the phases that formed for compositions with Ti > 48 at. % (Figure 4) were directly responsible for the observed phase transformation behavior.

The transforming phases (R and B2, shown in Figure 4a), formed in the region between 50 at. % and 70 at. % Ti. This region corresponds very well with the B2−R phase transforming compositions confirmed by $R(T)$ screening (bounded by black dashed line). The room temperature phase is R-phase since its transformation temperature (R_s) is above room temperature. The compositional area outside the phase transforming region showing high peak intensity belongs to B2 phase. The transformation temperature of the B2 phase in this composition range does not transform on cooling up to -20 °C (R(T) limit), but they may potentially transform to martensite phase at lower temperatures (<-20 °C). The high peak intensity in the Ti poor side (<48 at. %) is also attributed to fcc-(Au, Ni) phase and the Ti_3Ni_4 phase. The peak position of the fcc-(Au, Ni) solid-solution phase shifted due to a change in lattice constants, which changes as a function of composition. A large change in lattice constant with a change in composition is expected due to a significant difference in the atomic radii of Au and Ni. For example the (111) peak position of the fcc-(Ni, Au) solid solution shifts from $2\theta = 38.2°$ for 100 at. % Au[30] to $2\theta = 44°$ for 100 at. % Ni.[31] The Ti_3Ni_4 phase also contributes to the peak intensity profile since one of the two prominent diffraction peaks ($2\theta = 43.3°$ (21-2) and $2\theta = 42.5°$ (140)) for this phase appears close or at the same diffraction angle. The composition range with high peak intensity due to these phases shrunk with increasing annealing temperature, suggesting that their stability is suppressed with high annealing temperature.

The Ti_3Au phase (Figure 4b) formed for Ti > 49 at. % in all materials libraries. The intensity level increases toward high Ti and Au content. For higher annealing temperatures, it still formed at the Ti-rich side, but the peak intensity decreased for compositions close to 50 at. % Ti. The phase transforming composition regions (B2−R, B2−R−B19′, and B2−B19) are found within the Ti_3Au phase stability region. The decrease of peak intensity of Ti_3Au phase near 50 at. % Ti corresponds with the appearance of the B2−B19 phase transformation for materials libraries annealed at 600 and 700 °C.

The $TiAu_2$ phase (Figure 4c) mainly formed in the vicinity of 40−60 at. % Ti and above 10 at. % Au for the materials library annealed at 500 °C. After annealing at higher temperatures the phase stability region slightly shrunk but remained in the same vicinity. Annealing at high temperatures also resulted in the appearance of the B2−B19 type transformation within this composition region. The peak breadth of a neighbor peak at $2\theta = 40.9°$ belonging to the (111) B19 phase also contributes partially to the peak intensity plot.

The $TiAu_4$ phase (Figure 4d) formed over the composition range of 25−60 at. % Ti and above 10 at. % Au for the materials library annealed at 500 °C. It is interesting to note that it formed even for Ti-rich (>50 at. %) compositions. Previously it was determined that in a Ti/Au thin film diffusion couple Ti atoms diffuse faster into the Au layer than vice versa during annealing.[32,33] Therefore, the diffusing Ti atoms will be surrounded immediately with more Au atoms leading to the formation of Au-rich phases, such as $TiAu_4$ (similarly for $TiAu_2$). Annealing at higher temperatures suppresses the phase stability and it completely disappeared for Ti > 40 at. % for the materials library annealed at 700 °C. The decrease in the phase stability with increasing annealing temperature led to the appearance of B2−B19 phase transformation. The (111) fcc-(Au, Ni) diffraction peak also appears as neighbor peak and partially contributes to the peak intensity profile.

The Ti_2Ni phase (Figure 4e) formed for a composition region with >50 at. % Ti and <10 at. % Au. The peak intensity is very low for the materials library annealed at 500 °C indicating that only a small amount formed. The phase stability region of Ti_2Ni is found partially within the phase transforming composition region. The peak intensity increased and the phase stability region widened with increasing annealing temperature. These changes correspond very well with the appearance of B2−R−B19′ phase transformation.

The peak intensity profiles of the other phases that did not directly influence the phase transforming composition range are Figure 4f) Ti_3Ni_4 and fcc-(Ni, Au) phases, Figure 4g) $TiNi_3$, Figure 4h) fcc-Ni and Figure 4i) α-Ti and fcc-Au. The presence of Ti_3Ni_4, $TiNi_3$, fcc-(Ni, Au) and fcc-Ni forms the left boundary where phase transformation was not confirmed. The phase transforming composition range is bounded on the right side due to the formation of α-Ti phase.

Relationship between Phase Formation and the Phase Transforming Region. Figure 5 illustrates the relationships between phase formation and the resulting functional properties of Ti−Ni−Au thin films. There is no ternary phase diagram published for this system, so the binary sections[34−36] were adapted in the figure. Inside the composition diagram the phase transforming composition boundaries were drawn with respect to the $R(T)$ screening results shown in Figure 3. The Ti−Ni and the Ti−Au sides form a lot of intermetallic compounds while the Ni−Au side only forms the fcc solid-solution with the appearance of Ni-rich, Au-rich, and mixed fcc phases. B2 phases (the parent phase responsible for the reversible phase transformation observed in these alloys) are nominally formed at B2−$Ti_{50}Ni_{50}$ (M_s < 80 °C) and B2−

dx.doi.org/10.1021/co5000745 | ACS Comb. Sci. 2014, 16, 678−685

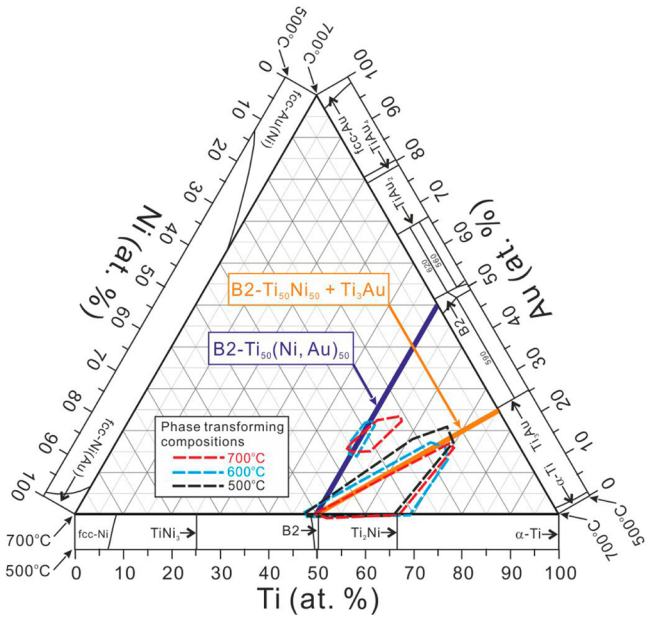

Figure 5. Schematic composition−structure−property diagram showing the phase transformation behavior with respect to composition and the equilibrium phases of binary compositions on each side. Two lines are shown pertaining to the formation of B2−Ti_{50}(Ni, Au)$_{50}$ solid-solution (blue line) and the two-phase (B2−$Ti_{50}Ni_{50}$+Ti_3Au) mixture (orange line). Binary sections were adapted from ref 34 for Ti−Ni, ref 35 for Ti−Au, and ref 36 for Ni−Au in the temperature range of 500−700 °C.

$Ti_{50}Au_{50}$ ($M_s \approx 600$ °C). According to previous work on Ti−Ni−Au bulk alloys[4] the elements Ni and Au can be substituted with each other in order to form the B2−Ti_{50}(Ni, Au)$_{50}$ solid-solution line (dark blue line in Figure 5). The transformation temperatures increase as Ni is substituted with Au, while keeping Ti at 50 at. %. A corresponding change in the martensite product structure is also expected: where <10 at. % Au the B19′ monoclinic or R trigonal phase will form and >10 at. % the B19 orthorhombic martensite will form. The B2−B19 phase transforming compositions is located along this line and between 15 at. % and 23 at. % Au. This is consistent with Au substituting for Ni in the B2 phase. Furthermore, this explains the appearance of B19 orthorhombic martensite and the increase of transformation temperatures, both of them are known effects in Ti_{50}(Ni, Au)$_{50}$ bulk SMA.[4] However, between 5 at. % and 15 at. % Au, phase transformation was not confirmed and for <5 at. % Au the line passes through the B2−R−B19′phase transformation boundary. The B2 phase (Figure 4a) is also found in this range but phase transformation was not confirmed. Phase transformation could be below the lower limit (-20 °C) of the R(T) measurement, or the B2 phase is completely stabilized.

The orange line in Figure 5 connects the B2−$Ti_{50}Ti_{50}$ and the Ti_3Au phase. Along this line the atomic ratio is exactly equal to 1:1 and 3:1 for Ti:Ni and Ti:Au, respectively. Therefore, this line could be regarded as a quasi-binary phase consisting of Ti_3Au (Ti:Au ratio of 3:1) and B2−$Ti_{50}Ni_{50}$ phase (Ti:Ni ratio of 1:1). This line forms the left boundary of the phase transforming composition region that shows B2−R and B2−R−B19′phase transformations. The compositions to the right side of the quasi-binary line have excess Ti and this leads to formation of Ti_3Au, Ti-rich (>50 at. %) B2−TiNi, and Ti_2Ni mix phases. The Ti-rich B2−TiNi phase is responsible for the B2−R and B2−R−B19′ phase transformations confirmed by R(T) screening. Whereas on the left side of the orange line, after the Ti_3Au phase formed then the remaining composition have excess Au and less Ti (Ni is balance). This explains the formation of Ti-poor (<48 at. %) B2−TiNi (Figure 4a) and Au-rich phases, such as $TiAu_2$ (Figure 4c) and $TiAu_4$ (Figure 4d). The Ti-poor B2−TiNi phase may potentially transform below the measurement temperature limit (-20 °C) of R(T) screening or may not transform at all due to a completely stabilized B2 phase. To form the B19 martensite at least 10 at. % Au has to be substituted for Ni in the B2−TiNi lattice,[4] thus within this composition range the B2−B19 transformation was not confirmed because not enough Au was substituted for Ni in the B2−TiNi lattice.

Compared to other Ti−Ni−X (X = Cu,[22] Pd,[14] Hf[21]) materials libraries prepared by thin film combinatorial synthesis and characterized by high-throughput experimentation, the appearance of two separate phase transforming composition regions in Ti−Ni−Au is the most significant difference. This is attributed to the difference in the alloying scheme for each materials library. The region undergoing B2−B19 transformation in Ti−Ni−Au is comparable to Ti−Ni−Pd where Au and Pd are preferentially substituted for Ni. The transformation temperatures increase with increasing amount of Au or Pd, but to achieve a high transformation temperature in Ti−Ni−Au, it requires higher annealing temperature. When compared to Ti−Ni−Cu, the B2−B19 transformation in Ti−Ni−Au have higher transformation temperatures. However, the composition range undergoing B2−B19 transformation is significantly narrower when compared to Ti−Ni−Cu. Therefore, the Ti−Ni−Au SMA system investigated in this study could be considered as a viable SMA for high temperature applications, but requires more stringent composition control and annealing condition.

Comparison of Results from Ti−Ni−Au Thin Film Materials Libraries with Bulk Ti−Ni−Au SMA. The Au content dependence of transformation temperatures determined in bulk Ti_{50}(Ni, Au)$_{50}$ SMAs is shown in Figure 6 (black

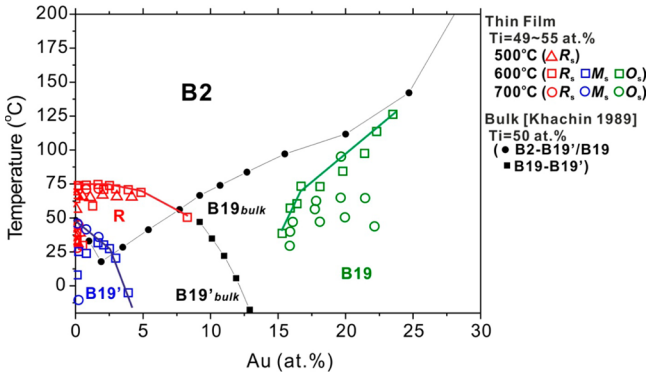

Figure 6. Au content dependence of transformation temperatures in thin film and bulk[4] Ti−Ni−Au SMA.

symbols).[4] The addition of Au (<2.5 at. %) first lowers the transformation temperature but with further addition of Au (>2.5 at. %) the transformation temperatures increase. The boundaries between the different martensite products are also shown. They change from B19′ to B19 at around 8 at. % Au. With increasing Au addition, the phase transformation boundary from B19 to B19′ decreases strongly in favor of

dx.doi.org/10.1021/co5000745 | ACS Comb. Sci. 2014, 16, 678−685

B19 martensite. The B2−B19 transformation temperature increases with increasing Au content until complete substitution, which is $Ti_{50}Au_{50}$ (not shown in Figure 6).

In comparison the transformation temperatures for thin films with Ti ≈ 49−55 at. % are plotted. The transformation temperatures of Ti−Ni−Au SMA thin films confirmed in this study have lower transformation temperatures compared to their bulk alloy counterpart of the same composition. This could be attributed to the combined influence of B2-phase matrix composition, precipitates, substrate constraint, and size effects on the phase transformation characteristics. In $Ti_{50}Ni$ binary SMA the Ni or Ti content of the B2-phase has a very strong influence on the transformation temperature, where M_s decreases by 83 K/at. % of excess Ni (>50 at. %) was reported.[37] Presence of physical boundaries, such as large amount of precipitates, substrate constraint, and size, could act as obstacles to phase transformation that could also lead to lower transformation temperatures. For Au contents < 5 at. %, the transformation temperature to B19′ martensite decreases strongly. This coincides very well with bulk SMA. However, in contrast to the bulk data, transformation temperature did not increase again with higher Au content. Another obvious difference is the appearance of R phase in thin films with up to 8 at. % Au: this can be attributed to the smaller grain size of B2 phase in thin films compared to bulk. In thin films the physical boundaries, such as film thickness and the presence of large amounts of precipitates both contribute to formation of small grain sizes by annealing. In Ti−Ni base SMA thin films as grain size decreases the transformation of B2 to R phase is favored over B19′ phase.[38] For compositions between 8 at. % to 15 at. % Au, phase transformation was not confirmed in thin films. This is because of the formation of various phases, such as $TiAu_4$, $TiAu_2$, Ti_3Au, and fcc-(Au, Ni) phases, which consumes the Au atoms and leaving none (or very few) to substitute for Ni in B2−TiNi phase. This effectively stabilized the B2−TiNi phase, thus no phase transformation was confirmed by $R(T)$ measurements within the temperature range limit. Above 15 at. % Au the B19 martensite formed and gradually the transformation temperatures increased. Above 20 at. % Au the transformation temperatures approached the data for bulk SMA reaching >100 °C, making them candidate materials for high temperature applications. However, above 25 at. % Au, phase transformation was not confirmed in thin films and this is due to the formation of $TiAu_2$ phase.

CONCLUSIONS

Ti−Ni−Au thin film materials libraries made by combinatorial sputtering were annealed at 500, 600, and 700 °C for 1 h. High-throughput characterization techniques were employed to establish the composition-structure−functional properties revealing the important factors to obtain high transformation temperatures (M_s > 100 °C) in Ti−Ni−Au SMA thin films. The major conclusions are as follows: (1) Phase transformations of the annealed materials libraries were confirmed by $R(T)$ measurements and it revealed three types of phase transformation paths: a) B2-R (trigonal), b) B2-R-B19′(monoclinic), and c) B2-B19 (orthorhombic). The B2−R transformation was only found in the materials library annealed at 500 °C for 1 h, while all types of phase transformation paths were confirmed in the materials libraries annealed at 600 and 700 °C for 1 h. Among them only the compositions with Ti ≈ 50 at. % and Au > 20 at. % are high temperature SMA since they exhibited transformation start temperatures (O_s) > 100 °C. They undergo B2−B19 transformation path, which is consistent with results from bulk Ti−Ni−Au SMA. (2) Phase formation for materials libraries annealed at 500 °C, 600 °C and 700 °C for 1 h were examined by XRD analysis. The composition and annealing temperature dependence of phase formation strongly influenced the functional properties. For example with increasing annealing temperature the amount of $TiAu_4$ and Ti_3Au phases decreased along the $Ti_{50}(Ni, Au)_{50}$ composition line. Consequently, it led to the appearance of B2−B19 transformation, which exhibited high transformation temperatures. (3) Two separate regions of phase transforming composition boundaries were explained by two different alloying scenarios. The first region is related to the substitution of Au on Ni site to form B2−$Ti_{50}(Ni,Au)_{50}$ phase. This is the region that showed B2−B19 phase transformation and transformation temperatures increased with Au content. The second region is bounded by a quasi-binary composition line consisting of Ti_3Au and B2−TiNi phases. The composition to the right side of this line showed B2−R and B2−R−B19′ phase transformations. (4) Compared to published results of bulk $Ti_{50}(Ni, Au)_{50}$ SMA, the thin film ($Ti_{49-55}(Ni, Au)_{51-45}$ selected compositions) results in this study revealed (a) the appearance of R phase for Au < 8 at. %, (b) no phase transformation between 8 at. % and 15 at. % Au, (c) B2−B19 transformation was confirmed only between 15 at. % and 23 at. % Au, and (d) transformation temperatures are typically lower.

AUTHOR INFORMATION

Corresponding Authors

*E-mail: pio.buenconsejo@rub.de; pbuenconsejo@ntu.edu.sg.

*E-mail: alfred.ludwig@rub.de.

Present Address

‡P. J. S. Buenconsejo: Facility for Analysis Characterization Testing and Simulation (FACTS), School of Materials Science and Engineering, Nanyang Technological University, Singapore 639798.

Notes

The authors declare no competing financial interest.

ACKNOWLEDGMENTS

The authors would like to express their gratitude for support from the German Research Foundation (DFG) within the funding for the research unit FOR 1766 (High temperature shape memory alloys). The authors are grateful to Alan Savan for his technical support.

REFERENCES

(1) Miyazaki, S.; Fu, Y. Q.; Huang, W. M. *Thin Film Shape Memory Alloys: Fundamentals and Device Applications*; Cambridge University Press: Cambridge, 2009.

(2) Khachin, V. Martensitic transformation and shape memory effect in B2 intermetallic compounds of titanium. *Rev. Phys. Appl.* **1989**, *24*, 733−739.

(3) Donkersloot, H.; van Vucht, J. Martensitic transformation in Gold-Titanium, Palladium-Titanium and Platinum-Titanium alloys near the equiatomic composition. *J. Less-Common Met.* **1970**, *20*, 83−91.

(4) Khachin, V. N.; Pushin, V. G.; Sivokha, V. P.; Kondrat'yev, V. V.; Muslov, A.; Voronin, V. P.; Zolotukhin, Yu. S.; Yurchenko, L. I. Structure and properties of B2-Titanium compounds: Martensitic transformations. *Phys. Met. Metall.* **1989**, *67*, 125−135.

(5) Hsieh, S.; Wu, S. A study on ternary Ti-rich TiNiZr shape memory alloys. *Mater. Charact.* **1998**, *41*, 151−162.

(6) Abu Judom, D.; Thoma, P.; Kao, M.; Angst, D. ·High transformation temperature shape memory alloy: US Patent 5114504, 1992.
(7) Wu, S.; Wayman, C. M. Martensitic transformation and the shape memory effect in $Ti_{50}Ni_{10}Au_{40}$ and $Ti_{50}Au_{50}$ alloys. *Metallography* **1987**, *20*, 359−376.
(8) Kawamura, T.; Tachi, R.; Inamura, T.; Hosoda, H.; Wakashima, K.; Hamada, K.; Miyazaki, S. Effects of ternary additions on martensitic transformation of TiAu. *Mater. Sci. Eng.* **2006**, *A438−440*, 383−386.
(9) Declairieux, C.; Denquin, A.; Ochin, P.; Portier, R.; Vermaut, P. On the potential of $Ti_{50}Au_{50}$ compound as a high temperature shape memory alloy. *Intermetallics* **2011**, *19*, 1461−1465.
(10) Shi, H.; Delville, R.; Srivastava, V.; James, R. D.; Schryvers, D. Microstructural dependence on middle eigenvalue in Ti−Ni−Au. *J. Alloys Compd.* **2014**, *582*, 703−707.
(11) Quandt, E.; Halene, C.; Holleck, H.; Feit, K.; Kohl, M.; Schlossmacher, P.; Skokan, A.; Skrobanek, K. D. Sputter deposition of TiNi, TiNiPd, and TiPd films displaying the two-way shape memory effect. *Sens. Actuators A* **1996**, *53*, 434−439.
(12) Miyazaki, S.; Ishida, A. Martensitic transformation and shape memory behavior in sputter-deposited TiNi-base thin films. *Mater. Sci. Eng., A* **1999**, *273−275*, 106−133.
(13) Liu, Y.; Kohl, M.; Okutsu, K.; Miyazaki, S. A TiNiPd thin film microvalve for high temperature applications. *Mater. Sci. Eng., A* **2004**, *378*, 205−209.
(14) Zarnetta, R.; Savan, A.; Thienhaus, S.; Ludwig, A. Combinatorial study of phase transformation characteristics of a Ti−Ni−Pd shape memory thin film composition spread in view of microactuator applications. *Appl. Surf. Sci.* **2007**, *254*, 743−748.
(15) Mohanchandra, K. P.; Shin, D.; Carman, G. P. Deposition and characterization of Ti−Ni−Pd and Ti−Ni−Pt shape memory alloy thin films. *Smart Mater. Struct.* **2005**, *14*, S312−S316.
(16) Mohanchandra, K. P.; Shin, D.; Carman, G. P. Shape memory behavior of high temperature Ti−Ni−Pt thin films. *Thin Solid Films* **2006**, *515*, 1938−1941.
(17) Ludwig, A.; Zarnetta, R.; Hamann, S.; Savan, A.; Thienhaus, S. Development of multifunctional thin films using high-throughput experimentation methods. *Int. J. Mater. Res.* **2008**, *99*, 1144−1149.
(18) Thienhaus, S.; Hamann, S.; Ludwig, A. Modular high-throughput test stand for versatile screening of thin film materials libraries. *Sci. Technol. Adv. Mater.* **2011**, *12*, No. 054206.
(19) Takeuchi, I.; Long, C. J.; Famodu, O. O.; Murakami, M.; Hattrick-Simpers, J.; Rubloff, G. W.; Stukowski, M.; Rajan, K. Data management and visualization of X-ray diffraction spectra from thin film ternary composition spreads. *Rev. Sci. Instrum.* **2005**, *76*, No. 062223.
(20) Cui, J.; Chu, Y.; Famodu, O. O.; Furuya, Y.; Hatttrick-Simpers, J.; James, R. D.; Ludwig, A.; Thienhaus, S.; Wuttig, M.; Zhang, Z.; Takeuchi, I. Combinatorial search of thermoelastic shape memory alloys with extremely small hysteresis width. *Nat. Mater.* **2006**, *5*, 286−290.
(21) König, D.; Zarnetta, R.; Savan, A.; Brunken, H.; Ludwig, A. Phase transformation, structural and functional fatigue properties of Ti−Ni−Hf shape memory thin films. *Acta Mater.* **2011**, *59*, 3267−3275.
(22) Zarnetta, R.; Buenconsejo, P. J. S.; Savan, A.; Thienhaus, S.; Ludwig, A. High-throughput study of martensitic transformation in the complete Ti−Ni−Cu system. *Intermetallics* **2012**, *26*, 98−109.
(23) Buenconsejo, P. J. S.; Zarnetta, R.; König, D.; Savan, A.; Thienhaus, S.; Ludwig, A. A new prototype two-phase (TiNi)−(W) SMA system with tailorable thermal hysteresis. *Adv. Funct. Mater.* **2011**, *21*, 113−118.
(24) Zarnetta, R.; Takahash, R.; Srivastava, V.; Young, M. L.; Savan, A.; Furuya, Y.; Thienhaus, S.; Maaß, B.; Rahim, M.; Frenzel, J.; Brunken, H.; Chu, Y. S.; James, R. D.; Takeuchi, I.; Eggeler, G.; Ludwig, A. Identification of quaternary shape memory alloys with near zero thermal hysteresis and unprecedented functional stability. *Adv. Funct. Mater.* **2010**, *20*, 1917−1923.
(25) Liu, Y.; Huang, X. Substrate-induced stress and transformation characteristics of a deposited Ti−Ni−Cu thin film. *Philos. Mag.* **2004**, *84*, 1919.
(26) Huang, X.; Liu, Y. Some factors affecting the properties of sputter deposited NiTi-based shape memory alloy thin films. *Proc. SPIE* **2002**, *4934*, 210.
(27) Winzek, B.; Quandt, E. Zero hysteresis in shape memory Ti−Ni−X films (X = Cu, Pd) under constrain. *Mater. Res. Soc. Symp. Proc.* **2000**, *604*, 117.
(28) König, D.; Buenconsejo, P. J. S.; Grochla, D.; Hamann, S.; Pfetzing-Micklich, J.; Ludwig, A. Thickness-dependence of the B2−B19 martensitic transformation in nanoscale shape memory alloy thin films: Zero-hysteresis in 75 nm thick $Ti_{51}Ni_{38}Cu_{11}$ thin films. *Acta Mater.* **2012**, *60*, 306−313.
(29) Villars, P.; Cenzual, K. *Pearson's Crystal Data: Crystal Structure Database for Inorganic Compounds*, release 2012/13 (on DVD); ASM International: Materials Park, Ohio, USA.
(30) Ellner, M.; Kolatschek, K.; Predel, B. On the partial atomic volume and the partial molar enthalpy of aluminum in some phases with Cu and Cu_3Au structures. *J. Less-Common Met.* **1991**, *170*, 171−184.
(31) Mishima, Y.; Ochiai, S.; Suzuki, T. Lattice parameters of Ni(γ), Ni_3Al(γ'), and Ni_3Ga(γ') solid solutions with additions of transition and B-subgroup elements. *Acta Metall.* **1985**, *33*, 1161−1169.
(32) Tisone, T. C.; Drobek, J. Diffusion in thin film Ti–Au, Ti−Pd, and Ti−Pt couples. *J. Vac. Sci. Technol.* **1972**, *9*, 271−275.
(33) Martinez, W.; Gregori, G.; Mates, T. Titanium diffusion in gold thin films. *Thin Solid Films* **2010**, *518*, 2585−2591.
(34) Murray, J. L. Ni−Ti (Nickel−Titanium). In *Binary Alloy Phase Diagrams II*, Vol. 3; Massalski, T. B., Ed.; ASM International: Materials Park, Ohio, USA, 1990; pp 2874−2876.
(35) Murray, J. L. Au−Ti (Gold−Titanium). In *Binary Alloy Phase Diagrams II*, Vol.1; Massalski, T. B., Ed.; ASM International: Materials Park, Ohio, USA, 1990; pp 442−445.
(36) Wang, J.; Lu, X. G.; Sundman, B.; Su, X. Thermodynamic assessment of the Au−Ni system. *Calphad* **2005**, *29*, 263−268.
(37) Frenzel, J.; George, E. P.; Dlouhy, A.; Somsen, Ch.; Wagner, M.F.-X; Eggeler, G. *Acta Mater.* **2010**, *58*, 3444−3458.
(38) Buenconsejo, P. J. S.; Zarnetta, R.; Ludwig, A. The effects of grain size on the phase transformation properties of annealed (Ti/Ni/W) shape memory alloy multilayers. *Scr. Mater.* **2011**, *64*, 1047−1050.